Blocking of the Nicotinic Acetylcholine Receptor Ion Channel by Chlorpromazine, a Noncompetitive Inhibitor: A Molecular Dynamics Simulation Study

ARTICLE *in* THE JOURNAL OF PHYSICAL CHEMISTRY B · NOVEMBER 2006

Impact Factor: 3.3 · DOI: 10.1021/jp0604591 · Source: PubMed

7 AUTHORS, INCLUDING:

Yechun Xu
Shanghai Institute of Materia Medica
76 PUBLICATIONS **1,236** CITATIONS
SEE PROFILE

Francisco J Barrantes
Pontifical Catholic University of Argentina
219 PUBLICATIONS **4,380** CITATIONS
SEE PROFILE

Xiaomin Luo
Chinese Academy of Sciences
122 PUBLICATIONS **3,162** CITATIONS
SEE PROFILE

Weiliang Zhu
Shanghai Institute of Materia Medica
206 PUBLICATIONS **3,835** CITATIONS
SEE PROFILE

Blocking of the Nicotinic Acetylcholine Receptor Ion Channel by Chlorpromazine, a Noncompetitive Inhibitor: A Molecular Dynamics Simulation Study

Yechun Xu,[†] Francisco J. Barrantes,[‡] Jianhua Shen,[†] Xiaomin Luo,[†] Weiliang Zhu,[†] Kaixian Chen,[†] and Hualiang Jiang*[,†,§]

Drug Discovery and Design Centre, State Key Laboratory of Drug Research, Shanghai Institute of Materia Medica, Shanghai Institutes for Biological Sciences, and Graduate School, Chinese Academy of Sciences, 555 Zuchongzhi Road, Shanghai 201203, China, Instituto de Investigaciones Bioquímicas de Bahía Blanca and UNESCO Chair of Biophysics & Molecular Neurobiology, CC 857, B8000FWB, Bahía Blanca, Argentina, and School of Pharmacy, East China University of Science and Technology, Shanghai 200237, China

Received: January 23, 2006; In Final Form: July 30, 2006

A large series of pharmacological agents, distinct from the typical competitive antagonists, block in a noncompetitive manner the permeability response of the nicotinic acetylcholine receptor (nAChR) to the neurotransmitter acetylcholine. Taking the neuroleptic chlorpromazine (CPZ) as an example of such agents, the blocking mechanism of noncompetitive inhibitors to the ion channel pore of the nAChR has been explored at the atomic level using both conventional and steered molecular dynamics (MD) simulations. Repeated steered MD simulations have permitted calculation of the free energy (∼36 kJ/mol) of CPZ binding and identification of the optimal site in the region of the serine and leucine rings, at ∼4 Å from the pore entrance. Coulomb and the Lennard-Jones interactions between CPZ and the ion channel as well as the conformational fluctuations of CPZ were examined to assess the contribution of each to the binding of CPZ to the nAChR. The MD simulations disclose a dynamic interaction of CPZ binding to the nAChR ionic channel. The cationic ammonium head of CPZ forms strong hydrogen bonds with Glu262 (α), Asp268 (*β*), Glu272 (*β*), Ser276 (*β*), Glu280 (*δ*), Gln271 (*γ*), Glu275 (*γ*), and Asn279 (*γ*) nAChR residues. Finally, the conventional MD simulation of CPZ at its identified binding site demonstrates that the binding of CPZ not only blocks ion transport through the channel but also markedly inhibits the conformational transitions of the channel, necessary for nAChR to carry out its biological function.

Introduction

The nicotinic acetylcholine receptor (nAChR) is the best-characterized member of the pentameric Cys-loop superfamily of transmitter-gated ion channels that also includes the structurally related 5-hydroxytryptamine type 3 receptor, *γ*-aminobutyric acid type A and C receptors, and glycine receptors.[1−4] In embryonic receptor in muscle or in the adult form in electrocytes, nAChR have four homologous subunits in a stoichiometry $\alpha_2\beta\gamma\delta$ that are arranged pseudosymmetrically about a central ion-permeation pathway. Each subunit contains a large hydrophilic extracellular region where the ligand binds to, four transmembrane (TM) segments (M1−M4) which constitute the membrane-embedded region of the ion-permeation pathway, and a hydrophilic cytoplasmic region. The innermost ring of five M2 segments, one from each subunit, constitutes the walls of the nAChR ion pore.[5] Remarkably, a series of stratified rings in which a certain residue from one M2 interacts with the respective homologous residue from the other M2s align along the ion channel (Figure 1). From the extracellular side to the cytoplasmic side, these rings are located sequentially as outer

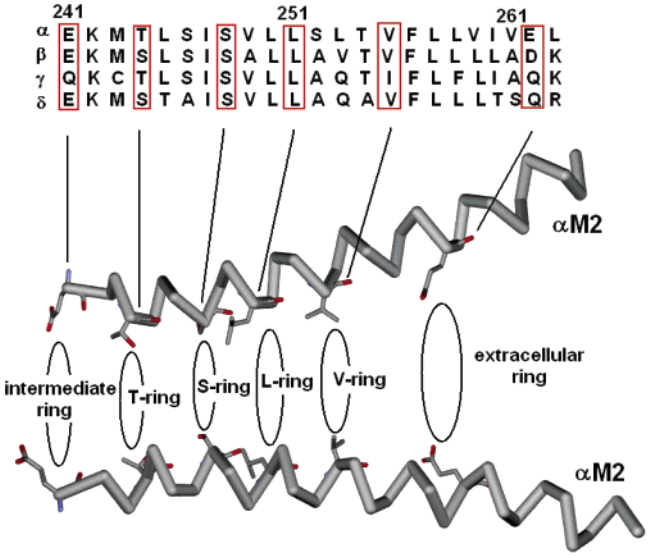

Figure 1. Composition and position of intermediate, threonine, serine, leucine, valine, and extracellular rings along the ion channel. The sequences and coordinates both derived from the structure from the PDB code 1OED.

or extracellular, valine, leucine, serine, and threonine, intermediate rings,[6] playing a key role when cations or other small molecules pass through the ion channel of the nAChR. The other TM segments, M1 and M3, form an intermediate region in contact with the five M2 segments and with the outermost

* To whom correspondence should be addressed to the Shanghai Institute of Materia Medica, Chinese Academy of Sciences, 555 Zu Chong Zhi Road, Zhangjiang Hi-Tech Park, Shanghai 201203, P. R. China. Phone: +86-21-50807188. Fax: +86-21-50807088. E-mail: hljiang@mail.shcnc.ac.cn.
[†] Chinese Academy of Sciences.
[‡] Instituto de Investigaciones Bioquímicas de Bahía Blanca and UNESCO Chair of Biophysics & Molecular Neurobiology.
[§] East China University of Science and Technology.

10.1021/jp0604591 CCC: $33.50
Published on Web 09/15/2006

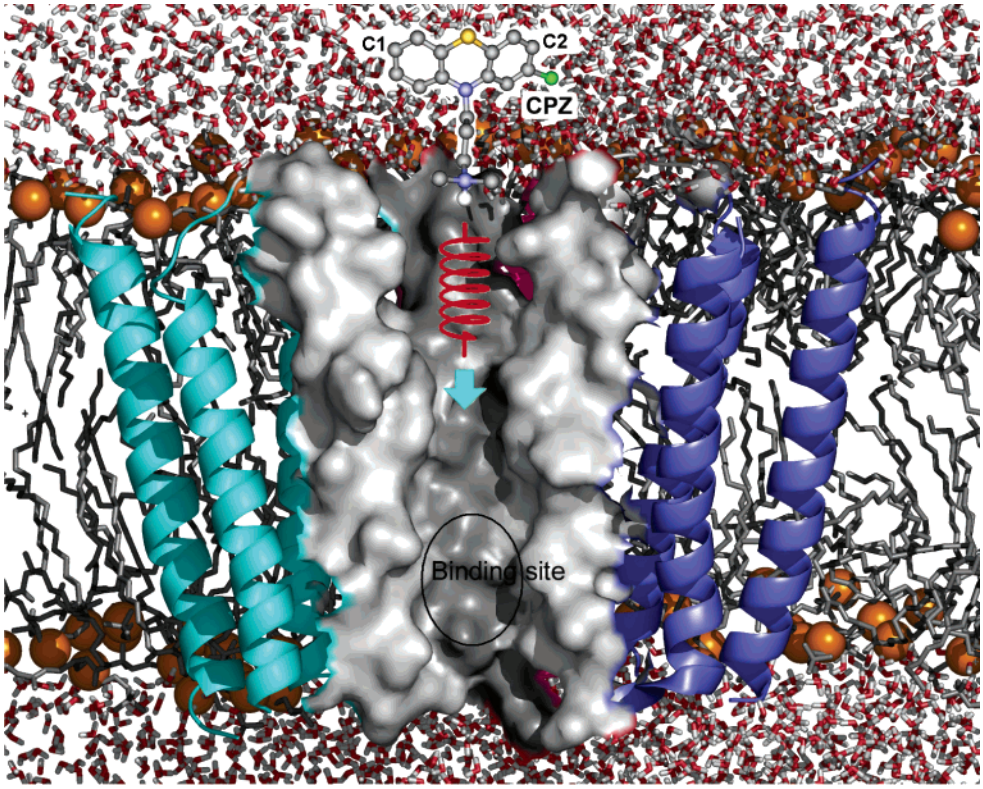

Figure 2. Model of the SMD simulation system. The TM nAChR region, comprising the ion channel proper, is shown as a ribbon. The surface is added to the M2 TM helix of each subunit. CPZ is shown as ball-and-sticks, pulled into the ion channel along the pore axis through a harmonic potential (spring and arrow). The phosphate atoms of lipid are shown as brown balls, and the other atoms of the lipid as well as water molecules are represented as sticks. The front half of the bilayer and the other two subunits have been removed to enable a view of the inner wall of the channel.

portion of five M4 segments which are directly in contact with the surrounding lipid phase.[5,7]

In addition to agonist recognition, the epiphenomenological function of the nAChR is the permeation of cations.[4] In general, four interconvertible functional states associated with the function of the nAChR have been characterized: the resting (closed) state; the open state; the fast-onset desensitized (closed or open) state; the slow-onset desensitized (closed or open) state.[3,8,9] Binding of agonists such as acetylcholine to the extracellular domain of the receptor triggers the opening of the ion channel located in the TM region and subsequently allows cations to flow through the central pore,[3] whereas noncompetitive inhibitors (NCIs), such as chlorpromazine (CPZ), inhibit the ion flux and enhance the desensitization rate of the receptor without significantly changing the apparent affinity for agonists.[10] It has been suggested that five M2 helices bend near the leucine ring (L-ring) and twist around the pore axis in response to the binding of acetylcholine, which results in a conformational transition from a closed to an open channel.[11] The binding of NCIs either *sterically* blocks ion flux by plugging the ionic channel or *allosterically* favors a conformation of the receptor in which the ion channel is closed and thus the ion flux is impeded too.[12,13] Therefore, the NCIs exert their pharmacological action through inhibition of the agonist-evoked ion flux, which results in a perturbation to the conformational equilibrium related to the four physiologically states of nAChR. Additionally, since the ion channel of the nAChR is the main binding target for NCIs, the labeling studies of NCI binding site have provided potentially useful tools for the structural identification of the components of the receptor.[14−19]

With the emergence of more accurate structures of the ligand binding domain (LBD), the ion channel, and even the entire receptor,[7,20−23] applications of molecular dynamics (MD) simulations in combination with other molecular modeling approaches have been performed to explore the dynamic conformations of LBD,[24,25] the interactions between agonist/antagonist and LBD,[26−30] conformational fluctuations of ion channel,[25,31−35] and the permeation of ions in the channel,[33,36] providing explanations for existing experimental results and extending our knowledge beyond what is accessible to current experimental techniques. Earlier modeling studies of CPZ and other NCIs were based on speculative models of the channel usually composed of the M2 TM helix only.[37−40] In the present work, MD simulations have been applied to investigate the blocking mechanism of CPZ to nAChR on the basis of the recently available cryoelectron microscopy structure of the whole nAChR TM domain.[7] Although the postulated binding site and binding affinity of CPZ to the ion channel of nAChR have been investigated in early experimental studies, there are still major issues to be resolved at the atomic level: What is the binding pathway of CPZ to its binding site near the cytoplasmic side of the ion channel? How could CPZ pass over the gating position with a large tail, the triple-ring of CPZ? What is the exact topology of CPZ at its binding site? How does CPZ exert its noncompetitive inhibition on the receptor? To arrive at answers to these questions, we pulled CPZ through the ion channel of the nAChR using steered MD (SMD) simulations, a well-used approach in studying the dynamic and kinetic processes of ligand−receptor binding and unbinding,[41−43] and subsequently used energy evaluations in combination with structural analyses to predict the optimal binding sites for CPZ that ultimately validate existing experimental data. Moreover, an extended 10-ns conventional MD (CMD) simulation on the CPZ-nAChR

channel complex revealed how CPZ exerts its noncompetitive inhibition on the function of the receptor.

Models and Methods

The setup of the simulation system, the ion channel of nAChR embedded into dipalmitoyl−phosphatidylcholine (DPPC) lipid bilayers, and simulation conditions have been described in our previous paper.[35] The cryoelectron crystallographic structure of the whole nAChR TM domain (PDB code, 1OED)[7] was inserted into a preequilibrated DPPC bilayer containing 512 lipid molecules. Consequently, more than 100 lipids were removed from the lipid bilayer to generate a suitable membrane system into which the TM domain of the nAChR could be embedded. The protein/DPPC system was then solvated in a bath of SPC water molecules.[44] The resulting system was submitted to energy minimization to remove unfavorable contacts and equilibrated for 1 ns with positional restraints on the protein atoms. Counterions were subsequently added to compensate for the net positive charge of the system. Finally, the total system comprised 80 287 atoms.

Water, lipids and protein were coupled separately to a temperature bath at 323 K using a coupling time of 0.1 ps.[45] The LINCS method[46] was used to constrain bond lengths, allowing an integration step of 2 fs. A constant pressure of 1 bar was applied independently in *x*, *y*, and *z* directions of the whole system with a coupling constant of 1.0 ps.[45] After 2-ns CMD simulation, CPZ was positioned at the extracellular side of the channel with its ammonium head pointing toward the channel pore. The previous simulation box was enlarged along the pore axis to cover the location of CPZ, and additional water molecules were filled into the box. Subsequently, an additional 1-ns CMD simulation was performed on this newly built simulation system. Afterward, CPZ was pulled through the channel pore along the pore axis from the extracellular side to the cytoplasmic side (Figure 2) starting with a snapshot extracted from the 1-ns simulation. When CPZ entered its optimal binding site as identified by structural analyses and energy calculations, an extended CMD simulation (10 ns) was run to explore the stability and motion of CPZ at the binding site. To ascertain common events occurring during the binding process of CPZ, the SMD simulation was repeated three times with different starting snapshots isolated from the 1-ns simulation trajectory. During all these SMD simulations, the pulling velocity was set at 0.05 Å·ps^{-1}, the spring-constants of the harmonic potential were set at 2.8 N·m^{-1}, and the pulling force was assigned to the ammonium head of CPZ.

The GROMACS simulation package[47,48] was employed for all these MD simulations, using the same parameters as described before.[35] The modified GROMOS87 force field[49] was applied for protein, and the lipid parameters adopted were those used in previous MD studies of lipid bilayers.[50−53] The geometry of CPZ was optimized at the HF/6-31G** level by the Gaussian 98 program,[54] and its partial atomic charges were subsequently determined using the ChelpG method[55] implemented in Gaussion98 with 6-31G** basis set. Topology file and other parameters for CPZ were generated using program PRODRG (http://davapc1.bioch.dundee.ac.uk/programs/prodrg/prodrg.html).[56] All the MD trajectory analyses were accomplished using facilities within the GROMACS package. The binding free energy of CPZ to the ion channel was calculated using the AutoDock3.05 scoring function.[57] Every 50 ps, the conformation of the ion channel and CPZ complex was extracted from the SMD trajectory for free energy calculation. LIGPLOT, a program for automatically plotting protein−ligand interactions, was adopted to analyze the hydrogen bonds and hydrophobic interactions between CPZ and the ion channel.[58] Structural diagrams were prepared using the PyMOL program (http://pymol.sourceforge.net/).

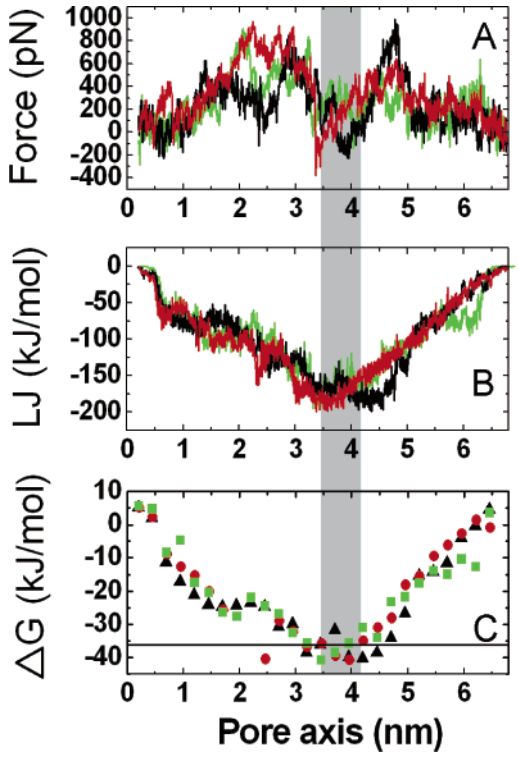

Figure 3. Recorded pulling force (A), the Lennard-Jones (LJ) potential between CPZ and the ion channel (B), and the binding free energy of CPZ evaluated by the AutoDock scoring function (C) versus positions along the pore axis in three SMD simulations. The different colors represent different SMD trajectories carried out under the same pulling velocity and direction but with different starting points.

Results

Entrance of CPZ Into Its Binding Site. To characterize the CPZ binding site of the nAChR and address the corresponding binding mechanism, SMD simulations were conducted by pulling CPZ along the pore axis of the nAChR channel to detect the motional behavior of CPZ through the ion channel. The zero point of the pore axis was set at the initial centroid of CPZ, and its positive direction is from top to bottom (Figure 2). Previous SMD simulation studies[42,59,60] have shown that the protein−ligand binding/unbinding mechanism may not be significantly affected by the pulling velocity under 0.1 Å·ps^{-1}, so we set the pulling velocity at 0.05 Å·ps^{-1} in our SMD simulations. As shown in Figure 3A, the recorded pulling force as a function of its position along the pore axis revealed that three repeated SMD simulations obtained a similar landscape of the force profile. In general, the pulling force was first averaged around zero. It then increased and reached the highest peak of the whole force profile after which the pulling force was reduced to form a trough and a second force peak followed. Finally, CPZ was passed through the entire ion channel, ref1ected in a decrease in the force with respect to the starting period. An analysis of the pulling force along the entire CPZ pathway through the ion channel leads to the conclusion that the position near 4 nm of the pore axis where the force trough is located is most likely to be the optimal binding site for CPZ.

The interaction potential between CPZ and the ion channel and the binding free energy of CPZ to the channel were

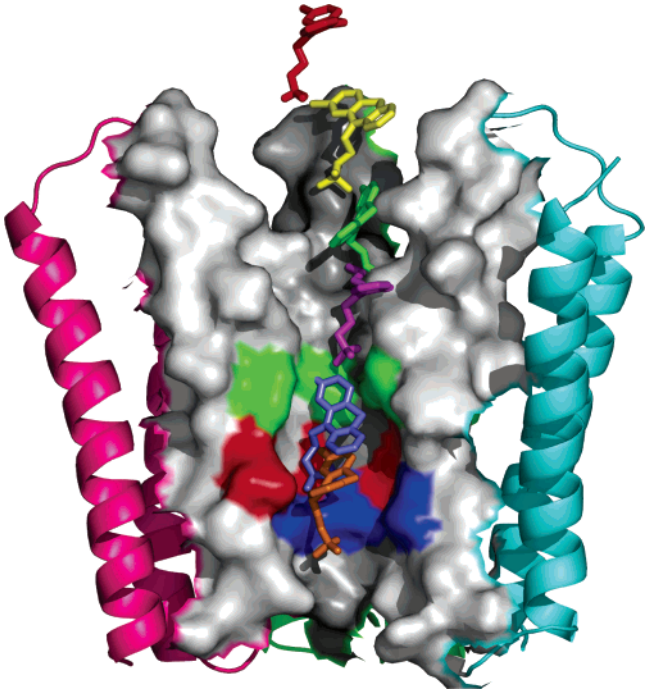

Figure 4. CPZ pathway to its binding site on the nAChR channel shown by a series of extracted snapshots of CPZ from one SMD trajectory. The nAChR ion channel is shown as a ribbon, and a surface is rendered to the M2 TM helix of each subunit. The positions of the V-, L-, and S-rings along the pore are colored green, red, and blue on the surface, respectively. CPZ is shown as sticks, and different colors represent different snapshots isolated from the SMD trajectory.

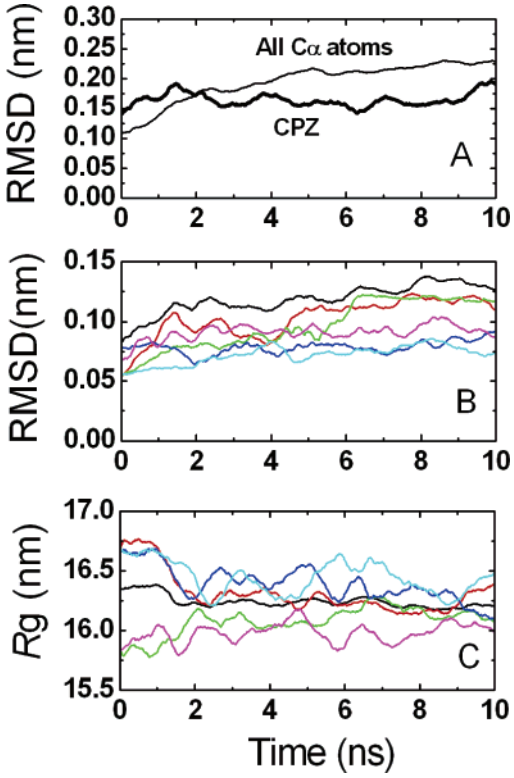

Figure 5. Time-dependent rmsds with respect to the starting structure and R_g for the ion channel or/and CPZ during the 10-ns CMD simulation. All the time series data were smoothed over 500-ps intervals. (A) Rmsds of C_α atoms of the ion channel and CPZ with fitting on all C_α atoms of the ion channel. (B) Rmsds of C_α atoms of M2(s). Two models were fitted, one corresponding to C_α atoms of M2 bundles of the five subunits (black) and the other corresponding to C_α atoms of the M2 of each individual subunit (red, green, blue, cyan, and magenta). (C) R_g for C_α atoms of $(M1-M3)_5$ (black) and each M1−M3 (red, green, blue, cyan, and magenta) relative to the axis of the ion channel.

calculated to identify the optimal binding site for CPZ. As shown in Figure 3B, the Lennard-Jones potential between CPZ and the ion channel decreases as the CPZ goes into the ion channel until it arrives at ∼4 nm of the pore axis. From this point to the end of the simulation, however, the potential begins to increase. A similar landscape was seen in the profile of the binding free energy of CPZ to the ion channel (Figure 3C), strongly suggesting that the position near 4 nm at the pore axis is a favorable location for CPZ binding. Furthermore, the profiles of the Lennard-Jones potential and the binding free energy obtained from the three repeated SMD simulations are very similar (Figures 3B and C), making the conclusion derived from these profiles more reliable. Therefore, the changes of the Lennard-Jones potential and the binding free energy both show that the optimal binding site for CPZ is located near 4 nm of the pore axis. Remarkably, the predicted binding free energy of CPZ to the potential binding site of nAChR is fully consistent with that derived from the experimental binding affinity (∼36 kJ/mol, black line in Figure 3C).[19] Interestingly, the experimental binding affinity was determined with CPZ bound to the ion channel in a desensitized state (purportedly in an open channel conformation) whereas the starting structure used in current simulations has been assumed to correspond to the channel in the resting, closed state. To examine the conformational state of the gate, the pore radii of the L-ring and the V-ring along the binding process of CPZ were calculated (Figure S1, Supporting Information). When CPZ reached its binding site within the channel pore, the pore radii of both the L-ring and the V-ring were found to be nearly 1 Å larger than those in the starting structure, suggesting that the channel is no longer in the closed state upon CPZ binding. In agreement with our observations, a paper that appeared after submission of this manuscript[61] suggests that the main changes in structure/orientation of the channel upon desensitization involve the solvent-accessible regions such as the ligand binding sites, with little if any changes in the TM region. Thus, conformational changes in the membrane-embedded domain of the nAChR induced by desensitization may be restricted to the rearrangement of side chains of the ion channel gate region. This may explain why the predicted binding free energy of CPZ obtained from the simulation—starting with a closed channel structure—is fully consistent with that derived from the experimental binding affinity determined with the ion channel in a desensitized state.

Figure 4 exhibits several typical snapshots of CPZ isolated from one SMD trajectory, which further confirms the reliability of the optimal binding site of CPZ to the nAChR as primarily identified by mapping the pulling force profile of CPZ moving along the receptor channel (Figure 3A), and subsequently confirmed by the Lennard-Jones potential and the binding free energy profiles between CPZ and the receptor (Figure 3B,C). Early experimental studies have inferred that the polar serine ring (S-ring) within the ion channel of the nAChR may be the preferred binding target for CPZ and the location of CPZ is most possibly in the axis of symmetry on the nAChR, in close proximity to all five chains of the receptor.[16,18,62,63] Besides the S-ring, the other two inner rings, the hydrophobic L-ring and the polar threonine ring, might also participate in the CPZ-binding site.[16] In our simulations, when CPZ was pulled into the position near 4 nm of the pore axis (orange color snapshot in Figure 4), the ammonium group of CPZ just passed over the S-ring and the triple-ring moiety of CPZ was located between

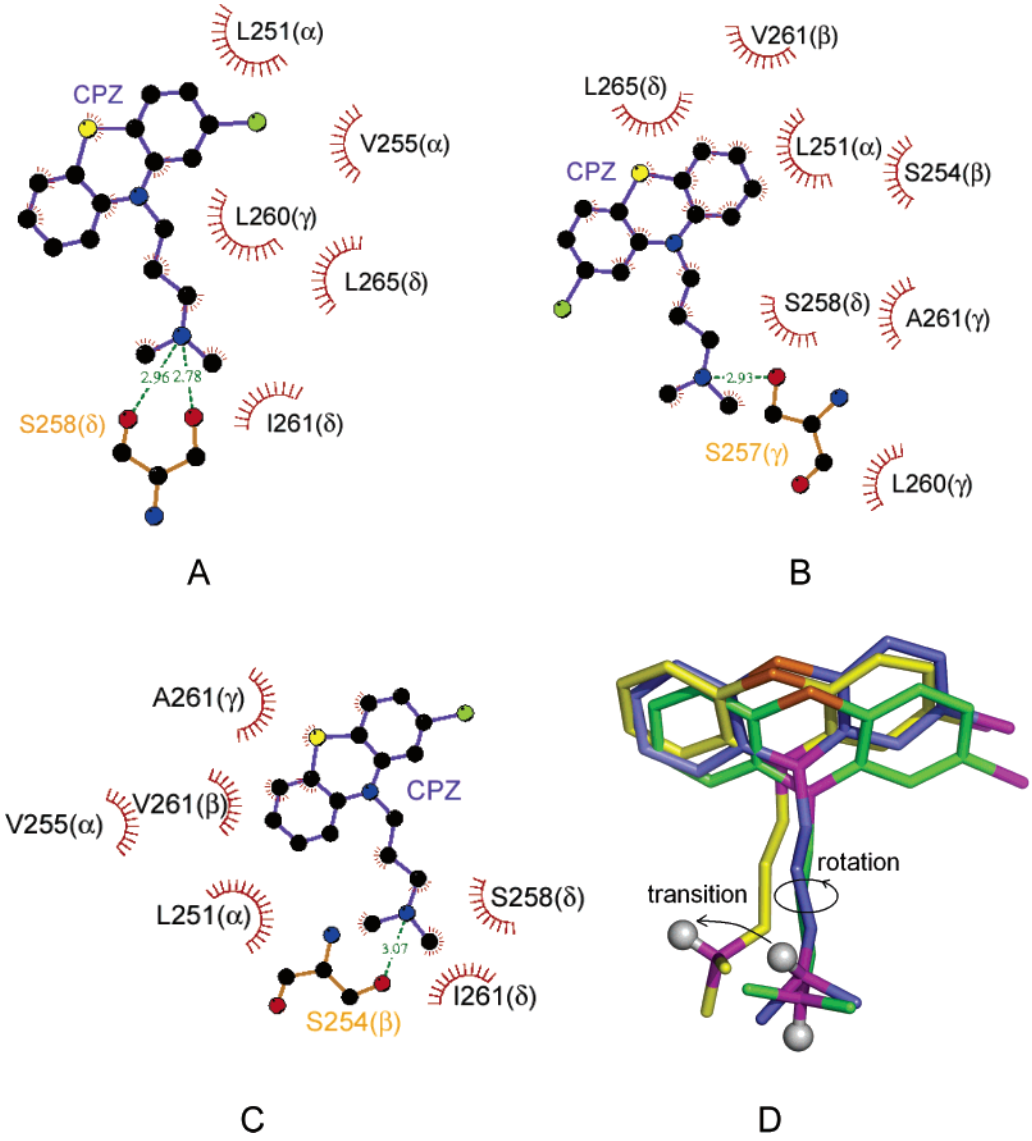

Figure 6. (A−C) Schematic representation of hydrogen bonds and hydrophobic interactions between CPZ and the ion channel at different snapshots extracted from the 10-ns equilibrium simulation. Dashed lines represent hydrogen bonds, and spiked residues form hydrophobic interactions with CPZ. (D) Superposition of CPZ from these three snapshots based on the fitted model of all C_α atoms of $(M1-M3)_5$. The hydrogen atom of CPZ is shown as a gray ball, and the other atoms are represented as sticks. The arrows show the switch directions of the CPZ ammonium group.

L-ring and S-ring. This is in accordance with the putative binding site of CPZ deduced from the early labeling studies.[16,18,62,63]

Equilibrium of CPZ at Its Binding Site. After the optimal binding site for CPZ was identified, an extended 10-ns CMD simulation was carried out to investigate the dynamic behavior of CPZ and the effects of CPZ binding on ion channel function. The root-mean-square deviation (rmsd) of CPZ was sustained at ∼1.6 Å throughout the whole 10-ns simulation duration (Figure 5A), demonstrating that CPZ was stable at its optimal binding site. Further analysis of the interactions between CPZ and the ion channel indicated that the stability of CPZ at its optimal binding can be mostly attributed to the formation of the hydrogen bonds and hydrophobic interactions between CPZ and residues near or belonging to the S- and L-rings. Three snapshots comprising these interactions are presented in Figure 6A−C. Obviously, the residues from each receptor subunit have the opportunity to interact with CPZ, which explains why CPZ labels four homologous chains of nAChR when it binds to the high-affinity binding site within the ion channel.[16,18,19,62,63] Most strikingly, the cationic ammonium head of CPZ formed electrostatic and hydrogen-bonding interactions with serines from different subunits during the 10-ns simulation, for example for a time with Ser258 of the δ subunit (Figure 6A) and Ser257 of γ subunit (Figure 6B). The superposition of CPZ from these three snapshots (Figure 6D) shows that the flexible bonds between the ammonium group and the triple-ring moiety of CPZ allows the cationic head to easily switch its orientation and thus dynamically contact serines from different subunits. This again explains why CPZ was able to label four homologous chains of nAChR at its binding site within the ion channel. Therefore, the triple-ring of CPZ acts as an anchor at the binding site of the nAChR, fixing the whole CPZ molecule (discussed below), whereas the cationic ammonium group swings around the channel wall, stimulating the serines through the making and breaking of hydrogen bonds (including electrostatic interaction).

In addition to the fluctuations of CPZ, the dynamic behavior of the nAChR ion channel during the 10-ns CMD simulation was also monitored. The C_α rmsd of the whole ion channel reached ∼2 Å after the first 2 ns and then remained constant until the end of the simulation (Figure 5A). Particular attention was paid to the dynamic behavior of M2 TM helix bundle, since it constitutes the inner wall of the channel and its conformational changes or motions directly affect the shape of the channel pore.

All the C_α rmsds of M2, as shown in Figure 5B, were below 1.5 Å throughout the entire 10-ns simulation duration, suggesting that M2 fluctuations are very small and that this inner ring for the most part holds its initial conformation. The radius of gyration (R_g) of M1−M3, calculated on the *xy* plane of the channel perpendicular to the pore axis, also underwent small changes, and the R_g of each M1−M3 approached that of $(M1-M3)_5$ from 2 to 10 ns (Figure 5C). Thus, the fluctuations of C_α rmsd and R_g suggest that the conformation of the ion channel remains practically the same during this 10-ns CMD simulation with the binding of CPZ to the ion channel.

Discussion

In this study, MD simulations and energy calculations have been applied to investigate the blocking mechanism of CPZ to the nAChR at the atomic level. Similar studies have been carried out before. The first atomic model of CPZ binding into the inner wall of nAChR was presented by Furois-Corbin et al. by adopting assumptions derived from the results of labeling experiments.[37] The energy profile of CPZ along the ion pore of nAChR was calculated by Tikhonov et al. using a restrained Monte Carlo minimization method.[38] Recently, Ortells and Barrantes docked CPZ into the ion channel to obtain the interaction pattern between CZP and the channel.[10] All these studies suggested that the hydrophobic moiety of CPZ prefers binding to the L-ring whereas its charge group reaches polar side chains of S-ring and T-ring, which is consistent with our observations described above. However, previous studies were based on speculative models of the channel which usually include M2 TM helices only, whereas in our current studies the newly available cryoelectron microscopy structure of the whole TM domain of nAChR was applied. Moreover, our study not only identifies the binding topology of CPZ within the ion channel but also explores the *binding pathway* of CPZ to its binding site with a large tail (the triple-ring of CPZ) and compares the conformation changes of nAChR in the presence and absence of CPZ. The details are discussed below.

The optimal binding sites for CPZ identified by structural and energetic analyses of SMD trajectories are in agreement with the experimental evidence and previous modeling studies, enabling us to postulate a detailed binding mechanism of CPZ on the basis of the simulation results. The recorded pulling force profiles indicate that CPZ has to overcome a high force peak before arriving at its optimal binding site at ~4 nm of the pore axis (Figure 3A). However, the Lennard-Jones potential between CPZ and the ion channel always favors the entrance moving of CPZ into its binding site (Figure 3B), which excludes the possibility that this high force peak is assigned to forming/breaking the Lennard-Jones interactions. Force profiles (Figure 3A) indicate that a force peak occurred when CPZ had just entered the channel vestibule (yellow snapshot in Figure 4). Structural analysis suggests that the cationic ammonium head of CPZ forms strong hydrogen bonds with receptor residues such as Glu262 (α), Asp268 (*β*), Glu272 (*β*), Ser276 (*β*), Glu280 (*δ*), Gln271 (*γ*), Glu275 (*γ*), and Asn279 (*γ*). The force peak most probably originated in the breaking of these hydrogen bonds. To further address this possibility, the short-range Coulomb interaction potential which mainly reflects the hydrogen-bonding interactions between CPZ and the ion channel versus the three SMD simulations was examined. The results are shown in Figure 7A. Obviously, there is a well on the Coulomb potential profile at the position of the entrance, i.e., at the vestibule of the pore. This is in agreement with the structural features of both CPZ and receptor, since the electrostatic

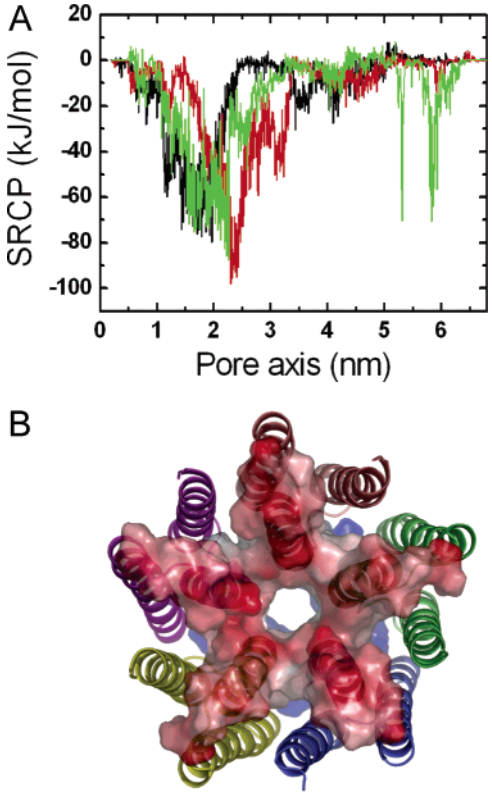

Figure 7. (A) Short-range Coulomb potential (SRCP) between CPZ and the ion channel versus position along the pore axis in three SMD simulations. (B) Top view of the ion channel as seen from the extracellular side, with subunits shown in different colors. The electrostatic potential surface of the five M2 TM helices is displayed together. Areas of positive potential are shown in blue, and those with negative potential are in red.

potential around the entrance is negative (Figure 7B), attracting the positively charged cationic head of CPZ. Accordingly, the strong Coulomb interactions may act as a guide to allure CPZ into the ion channel.

Although CPZ formed strong Coulomb interactions with the vestibule of the pore, the calculated binding free energy profile of CPZ to the ion channel indicated that the position corresponding to the highest binding affinity for CPZ is located at the optimal binding site near the cytoplasmic side of the ion channel rather than at the entrance (Figure 3C). One question arises is how could CPZ escape the Coulomb potential well at the entrance to reach the optimal binding site? As mentioned above, the Lennard-Jones interactions favor CPZ continuing along the channel, which partially compensates the energy loss due to the breaking of Coulomb interactions. Another important factor facilitating the movement of CPZ might arise from the contribution of the inherent flexibility of CPZ itself. The angle between the channel pore axis and the axis passing through C1 and C2 carbon atoms of CPZ (see Figure 2 for the positions of these two atoms), reflecting the orientations of the triple-ring of CPZ inside the channel, was calculated along the three SMD trajectories. The result is shown in Figure 8. The initial value of the angle is ~100°, demonstrating that the triple-ring is almost perpendicular to the pore axis. As CPZ moves further into the ion channel, the value of the angle fluctuates dramatically, indicating that the triple-ring of CPZ frequently changes its orientation during CPZ moves toward the binding site. This is also reflected by the typical snapshots isolated from the SMD trajectories (Figure 4). It is thus postulated that the flexibility of CPZ, in particular the orientation switches of the triple-ring, enables CPZ to break the Coulomb interactions mainly formed

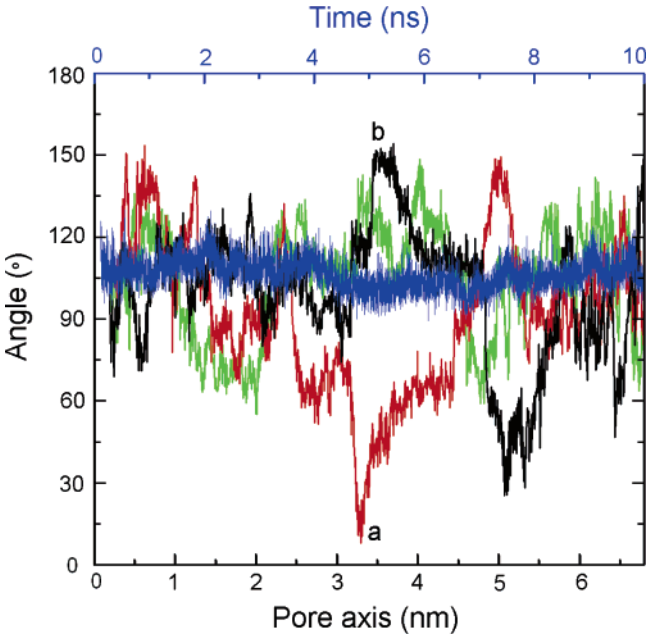

Figure 8. Angle between channel pore axis and the axis passing through C1 and C2 as a function of the position along the pore axis during the three SMD simulations (black, red, and green lines) and as a function of time during the 10-ns CMD simulation (blue line). C1 and C2 are two carbon atoms in the three-triple of CPZ as shown in Figure 2.

between the ammonium head of CPZ and the residues at the ion channel entrance and thus keep moving. Finally, water molecules may also help CPZ to overcome the barrier caused by the Coulomb interactions between CPZ and the vestibule of the channel. The short-range Coulomb potential shown in Figure 7A was obtained by taking into account the direct electrostatic interaction between CPZ and the channel without considering the solvent effects. There is one hydrogen atom in the ammonium head of CPZ, which is prone to form a hydrogen bond with water, thus making it possible to screen the Coulomb interactions mainly formed between the ammonium head of CPZ and the polar residues at the ion channel entrance. Although the pulling velocity applied in this study is low (0.05 Å·ps^{-1}), the simulated binding of CPZ to the ion channel is still much faster than the physiological process. The much slower binding process of CPZ under the physiological condition as well as the large space near the channel vestibule enables more water molecules to surround CPZ when it enters the vestibule. Because of the evident dynamic character of water molecules in the vicinity of the vestibule, entropic effects of these molecules may also play a significant role in helping CPZ to move further into its binding site within the channel. Water molecules may therefore provide both enthalpic and entropic contributions to the binding of CPZ into the channel.

Additionally, the orientation changes of the triple-ring of CPZ would also help CPZ to pass over the gating positions without causing significant force increase (Figure 3A). Figure 8 shows that the orientation departure of the triple-ring from its initial state reaches its furthest position close to the optimal binding site. Structural examination of two typical snapshots corresponding to points a and b in Figure 8 reveal that the triple-ring is almost parallel to the pore axis at these two points (Figure 9A,B). Moreover, it also shows that two conformations can be adopted by the triple-ring when it is parallel to the pore axis: one is that shown in Figure 9A, the chlorine atom of CPZ pointing to the S-ring, and the other is the chlorine atom of CPZ pointing to the V-ring (Figure 9B). Thus, the conformational flexibility of CPZ allows it to easily pass through narrow regions of the ion channel such as the gate. In our previous paper we reported that the reorganization of the side chains suffices to break the side-to-side hydrophobic girdle of the gate within the course of nanoseconds.[35] Here we further show that the pore radii of the gate region (L- and V-rings) increase upon CPZ binding (Figure S1 in Supporting Information), thus also facilitating CPZ passage through the V-ring without requiring a high pulling force. Hence, both the inherent flexibility of CPZ and the dynamic fluctuations of the gate region contribute to the binding of CPZ with a large triple-ring to the ion channel.

After CPZ arrives at its optimal binding site, the orientation of the triple-ring recovers its initial state and this orientation is stably maintained throughout the whole 10-ns CMD simulation (blue line in Figure 8). The snapshot extracted from the 10-ns CMD simulations shows that in the binding site the triple-ring adopts an inclined conformation and interacts with residues of the L-ring whereas the ammonium head reaches the S-ring region (Figure 9C). As described above, the triple-ring of CPZ acts as an anchor, fixing the whole CPZ molecule at the binding site of the nAChR, whereas the cationic ammonium head swings around the channel wall, stimulating the residues through the making and breaking of hydrogen bonds (including electrostatic

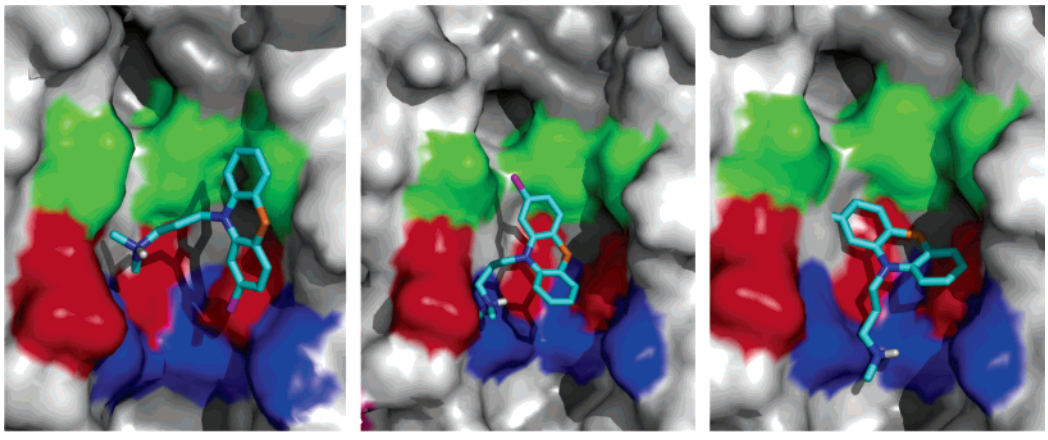

Figure 9. Locations of CPZ in the ion channel. The surface represents the inner part of the nAChR channel wall, and CPZ is shown as sticks. The positions of the V-ring, L-ring, and S-ring along the channel pore are colored green, red, and blue in the surface representation, respectively. (A) and (B) correspond to the snapshots of a and b in Figure 8, respectively. (C) One snapshot isolated from the 10-ns CMD trajectory.

interactions). This topology of CPZ at its binding site may partly explain why CPZ has a high affinity for the ion channel of the nAChR.[19]

The effect of CPZ binding on the ion channel was investigated by conformational examinations of the ion channel on the basis of an extended 10-ns CMD simulation. Asymmetrical and asynchronous translations of the M1−M3 TM segments of each subunit have been observed in our previous CMD simulation for the same cryoelectron crystallographic structure of nAChR channel as used in this work.[35] However, such motions have not been observed after CPZ binding to the ion channel, suggesting that the binding of CPZ largely inhibits the asymmetrical translation of each subunit. Additionally, the low rmsd of the M2 TM helix bundle indicate that the inner wall of the ion channel mainly keeps its initial conformation throughout the whole 10-ns simulation, at variance with the bending conformational change of M2 seen in our previous MD simulations on the empty, ion-permeable structure of the nAChR channel.[35] The observed hydrogen bonds and hydrophobic interactions between CPZ and the residues located in the M2 bundle, together with the luminal occupation of CPZ, may account for the conformational stability of M2 and even the entire channel. Hence, the binding of CPZ not only blocks the ion transport through the channel but also inhibits the large conformational transitions of the channel, exerting perturbations on conformational equilibria associated with the four physiologically states of nAChR.

Conclusions

The present MD simulations provide a novel dynamic view of the CPZ binding process to the ion channel of the nAChR at the atomic level. The consistency between the calculated binding free energy of CPZ to the binding site identified by MD simulations and that derived from the experimental affinity determination[19] encouraged us to address the possible binding mechanism of CPZ to the ion channel and characterize the exact topology of CPZ at its optimal binding site and its relationship to nAChR functions on the basis of our models and MD results, which cannot be addressed with currently available experimental techniques. The results enable us to conclude that Coulomb interactions of CPZ with the extracellular side of the ion channel act as a guide for CPZ entering into the ion channel. Subsequently, the increased hydrophobic interactions between CPZ and the ion channel together with entropy contribution originating in the intrinsic flexibility of CPZ act as driving forces to enable CPZ to overcome the hindrance along the channel pore and facilitate its continued movement toward its optimal binding site located near the L- and S-rings. When CPZ reaches its binding site, the triple-ring acts as a fixed anchor but the cationic ammonium head swings around the channel wall owing to the inherent flexibility of CPZ. Finally, compared with our previous MD simulation results on the functionally permeable nAChR channel,[35] the inhibitory effect of CPZ on the conformational transitions of the channel has been revealed; i.e., binding of CPZ may not only block ion transport but also restrict the conformational transition of the nAChR channel which is also a requisite for the receptor to exert its physiological functions. Thus, the experimentally comparable results provided by the present MD simulations as well as our previous MD study[35] greatly enhance our understanding of the structurally related functions of the nAChR and facilitate design of further experiments to refine receptor structure and function.

Acknowledgment. This work was supported by the State Key Program of Basic Research of China (Grant 2002CB512802), the National Natural Science Foundation of China (Grants 20372069, 29725203, and 20072042), the Basic Research Project for Talent Research Group from the Shanghai Science and Technology Commission, the Key Project form the Shanghai Science and Technology Commission (Grant 02DJ14006), the Key Project for New Drug Research from CAS, and UNS CONICET/FONCyT to F.J.B and NIH 1 R01 DA015389 grant.

Supporting Information Available: Pore radius of L-ring and V-ring versus positions along the pore axis in the binding process of CPZ. This material is available free of charge via the Internet at http://pubs.acs.org.

Abbreviations

CMD	conventional molecular dynamics
CPZ	chlorpromazine
LBD	ligand binding domain
nAChR	nicotinic acetylcholine receptor
NCIs	noncompetitive inhibitors
MD	molecular dynamics
R_g	radius of gyration
rmsd	root-mean-square deviation
TM	transmembrane
SMD	steered molecular dynamics

References and Notes

(1) Barnard, E. *Trends Biochem. Sci.* **1992**, *17*, 368.
(2) Hucho, F.; Weise, C. *Angew. Chem., Int. Ed.* **2001**, *40*, 3100.
(3) Karlin, A. *Nat. Rev. Neuronsci.* **2002**, *3*, 102.
(4) Barrantes, F. J. *The nicotinic acetylcholine receptor: current views and future trends*; Springer-Verlag: Berlin/Heidelberg and Landes, Georgetown, TX, 1998.
(5) Barrantes, F. J. *Curr. Opin. Drug Discuss. Dev.* **2003**, *6*, 620.
(6) Corringer, P.-J.; Le Novere, N.; Changeux, J.-P. *Annu. Rev. Pharmacol. Toxicol.* **2000**, *40*, 431.
(7) Miyazawa, A.; Fujiyoshi, Y.; Unwin, N. *Nature* **2003**, *423*, 949.
(8) Changeux, J.-P.; Edelstein, S. J. *Curr. Opin. Neurobiol.* **2001**, *11*, 369.
(9) Lena, C.; Changeux, J. P. *Trends Neurosci.* **1993**, *16*, 181.
(10) Ortells, M. O.; Barrantes, G. E. *Recept. Channels* **2001**, *7*, 273.
(11) Unwin, N. *Nature* **1995**, *373*, 37.
(12) Pascual, J. M.; Karlin, A. *J. Gen. Physiol.* **1998**, *112*, 611.
(13) Yu, Y.; Shi, L.; Karlin, A. *Proc. Natl. Acad. Sci. U.S.A.* **2003**, *100*, 3907.
(14) Arias, H. R. *Biochim. Biophys. Acta* **1998**, *1376*, 173.
(15) Arias, H. R. *Brain Res. Rev.* **1997**, *25*, 133.
(16) Revah, F.; Galzi, J.-L.; Giraudat, J.; Haumont, P.-Y.; Lederer, F.; Changeux, J.-P. *Proc. Natl. Acad. Sci. U.S.A.* **1990**, *87*, 4675.
(17) Heidmann, T.; Changeux, J.-P. *Biochemistry* **1986**, *25*, 6109.
(18) Giraudat, J.; Dennis, M.; Heidmann, T.; Haumont, P.-Y.; Lederer, F.; Changeux, J.-P. *Biochemistry* **1987**, *26*, 2410.
(19) Heidmann, T.; Oswald, R. E.; Changeux, J.-P. *Biochemistry* **1983**, *22*, 3112.
(20) Unwin, N. *J. Mol. Biol.* **2005**, *346*, 967.
(21) Brejc, K.; van Dijk, W. J.; Klaassen, R. V.; Schuurmans, M.; van Der Oost, J.; Smit, A. B.; Sixma, T. K. *Nature* **2001**, *411*, 269.
(22) Sixma, T. K.; Smit, A. B. *Annu. Rev. Biophys. Biomol. Struct.* **2003**, *32*, 311.
(23) Celie, P. H. N.; van Rossum-Fikkert, S. E.; van Dijk, W. J.; Brejc, K.; Smit, A. B.; Sixma, T. K. *Neuron* **2004**, *41*, 907.
(24) Henchman, R. H.; Wang, H. L.; Sine, S. M.; Taylor, P.; McCammon, J. A. *Biophys. J.* **2003**, *85*, 3007.
(25) Law, R. J.; Henchman, R. H.; McCammon, J. A. *Proc. Natl. Acad. Sci. U.S.A.* **2005**, *102*, 6813.
(26) Le Novere, N.; Grutter, T.; Changeux, J.-P. *Proc. Natl. Acad. Sci. U.S.A.* **2002**, *99*, 3210.
(27) Fruchart-Gaillard, C.; Gilquin, B.; Antil-Delbeke, S.; Le Novere, N.; Tamiya, T.; Corringer, P.-J.; Changeux, J.-P.; Menez, A.; Servent, D. *Proc. Natl. Acad. Sci. U.S.A.* **2002**, *99*, 3216.
(28) Schapira, M.; Abagyan, R.; Totrov, M. *BMC Struct. Biol.* **2002**, *2*, 1.
(29) Gao, F.; Bren, N.; Burghardt, T. P.; Hansen, S.; Henchman, R. H.; Taylor, P.; McCammon, J. A.; Sine, S. M. *J. Biol. Chem.* **2005**, *280*, 8443.

(30) Henchman, R. H.; Wang, H. L.; Sine, S. M.; Taylor, P.; McCammon, J. A. *Biophys. J.* **2005**, *88*, 2564.
(31) Sansom, M. S. P.; Adcock, C.; Smith, G. R. *J. Struct. Biol.* **1998**, *121*, 246.
(32) Law, R. J.; Forrest, L. R.; Ranatunga, K. M.; Rocca, P. L.; Tieleman, D. P.; Sansom, M. S. P. *Proteins: Struct. Funct. Genet.* **2000**, *39*, 47.
(33) Adcock, C.; Smith, G. R.; Sansom, M. S. P. *Eur. Biophys. J.* **2000**, *29*, 29.
(34) Law, R. J.; Tieleman, D. P.; Sansom, M. S. P. *Biophys. J.* **2003**, *84*, 14.
(35) Xu, Y. C.; Barrantes, F. J.; Luo, X. M.; Chen, K. X.; Shen, J. H.; Jiang, H. L. *J. Am. Chem. Soc.* **2005**, *127*, 1291.
(36) Smith, G. R.; Sansom, M. S. P. *Biophys. J.* **1997**, *73*, 1364.
(37) Furois-Corbin, S.; Pullman, A. *Biochim. Biophys. Acta* **1989**, *984*, 339.
(38) Tikhonov, D. B.; Zhorov, B. S. *Biophys. J.* **1998**, *74*, 242.
(39) Tikhonov, D. B.; Mellor, I. R.; Usherwood, P. N. R. *Biophys. J.* **2004**, *87*, 159.
(40) Barrantes, G. E.; Ortells, M. O.; Barrantes, F. J. *Neuropharmacology* **1997**, *36*, 269.
(41) Xu, Y. C.; Shen, J. H.; Luo, X. M.; Shen, X.; Chen, K. X.; Jiang, H. L. *Sci. China, Ser. B* **2004**, *47*, 355.
(42) Grubmuller, H.; Heymann, B.; Tavan, P. *Science* **1996**, *271*, 997.
(43) Izrailev, S.; Stepaniants, S.; Balsera, M.; Oono, Y.; Schulten, K. *Biophys. J.* **1997**, *72*, 1568.
(44) Berendsen, H. J. C.; Postma, J. P. M.; van Gunsteren, W. F.; Hermans, J. Interaction models for water in relation to protein hydration. In *Intermolecular Forces.*; Pullman, B., Ed.; Reidel: Dordrecht, The Netherlands, 1981; p 331.
(45) Berendsen, H. J. C.; Postma, J. P. M.; van Gunsteren, W. F.; DiNola, A.; Haak, J. R. *J. Chem. Phys.* **1984**, *81*, 3684.
(46) Hess, B.; Bekker, B.; Berendsen, H. J. C.; Fraaije, J. G. E. M. *J. Comput. Chem.* **1997**, *18*, 1463.
(47) Lindahl, E.; Hess, B.; van der Spoel, D. *J. Mol. Model.* **2001**, *7*, 306.
(48) Berendsen, H. J. C.; van der Spoel, D.; van Drunen, R. *Comput. Phys. Commun.* **1995**, *91*, 43.
(49) van Gunsteren, W. F.; Berendsen, H. J. C. *Gromos-87 manual*; Biomos BV: Nijenborgh 4, 9747 AG Groningen, The Netherlands, 1987.
(50) Tieleman, D. P.; Sansom, M. S. P.; Berendsen, H. J. C. *Biophys. J.* **1999**, *76*, 40.
(51) Berger, O.; Edholm, O.; Jahnig, F. *Biophys. J.* **1997**, *72*, 2002.
(52) Marrink, S. J.; Berger, O.; Tieleman, P.; Jahnig, F. *Biophys. J.* **1998**, *74*, 931.
(53) Tieleman, D. P.; Berendsen, H. J. C.; Sansom, M. S. P. *Biophys. J.* **1999**, *76*, 1757.
(54) *Gaussian 98*, revision A.4; Gaussian: Pittsburgh, PA, 1998.
(55) Breneman, C. M.; Wiberg, K. B. *J. Comput. Chem.* **1990**, *11*, 361.
(56) Van Aalten, D. M. F.; Bywater, R.; Findlay, J. B. C.; Hendlich, M.; Hooft, R. W. W.; Vriend, G. *J. Comput. Aided Mol. Des.* **1996**, *10*, 255.
(57) Morris, G. M.; Goodsell, D. S.; Halliday, R. S.; Huey, R.; Hart, W. E.; Belew, R. K.; Olson, A. J. *J. Comput. Chem.* **1998**, *19*, 1639.
(58) Wallace, A. C.; Laskowski, R. A.; Thomton, J. M. *Protein Eng.* **1995**, *8*, 127.
(59) Xu, Y. C.; Shen, J. H.; Luo, X. M.; Silman, I.; Sussman, J. L.; Chen, K. X.; Jiang, H. L. *J. Am. Chem. Soc.* **2003**, *125*, 11340.
(60) Shen, L. L.; Shen, J. H.; Luo, X. M.; Cheng, F.; Xu, Y. C.; Chen, K. X.; Arnold, E.; Ding, J. P.; Jiang, H. L. *Biophys. J.* **2003**, *84*, 3547.
(61) Hill, D. G.; Baenziger, J. E. *Biophys. J.* **2006**, *91*, 705.
(62) Giraudat, J.; Dennis, M.; Heidmann, T.; Chang, J.-Y.; Changeux, J.-P. *Proc. Natl. Acad. Sci. U.S.A.* **1986**, *83*, 2719.
(63) Giraudat, J.; Gali, J.; Revah, F.; Changeux, J.-P.; Haumont, P.-Y.; Lederer, F. *FEBS Lett.* **1989**, *253*, 190.